Hindawi
Shock and Vibration
Volume 2022, Article ID 8154492, 12 pages
https://doi.org/10.1155/2022/8154492

Research Article

Feature Extraction of Weak-Bearing Faults Based on Laplace Wavelet and Orthogonal Matching Pursuit

Lei Hou,[1,2] **Junxiao Zhao**,[1] **Shiwei Dun**,[3] **Yufeng Cai**,[3] **Yang Yang**,[2] **Junzhi Xu**,[1] **and Chuanzong Sun**[4]

[1]*School of Astronautics, Harbin Institute of Technology, Harbin 150001, China*
[2]*Applied Mechanics and Structure Safety Key Laboratory of Sichuan Province, School of Mechanics and Engineering, Southwest Jiaotong University, Chengdu 610031, China*
[3]*Factory of Xiang Yang Hang Tai Power Machinery, Xiangyang 441000, China*
[4]*School of Mechanical Engineering, Shenyang University of Technology, Shenyang 110870, China*

Correspondence should be addressed to Lei Hou; houlei@hit.edu.cn

Received 2 September 2021; Revised 5 January 2022; Accepted 29 January 2022; Published 20 March 2022

Academic Editor: Dario Richiedei

The transient impact component of early bearing faults is not obvious, and the traditional basis function expansion method is poor in feature extraction under strong noise conditions. In this paper, a transient feature extraction technique is proposed based on Laplace wavelet and orthogonal matching pursuit algorithm and combined with sparse representation theory. First, the overcomplete and redundant Laplace wavelet dictionary is adopted to represent vibration signals in a sparse way. Then the Hilbert resonance demodulation method is employed to obtain the envelope spectrum of sparse representation signal. Finally, the coefficient calculation problem of sparse representation is solved by orthogonal matching pursuit (OMP) algorithm. Simulation examples and experimental example are used to examine the performance of the proposed method. The results show that the weak-bearing faults feature extraction can be effectively realized since the transient shock component can be identified. Furthermore, the effectiveness of the proposed method is verified by the cyclic multishock simulated signals as well as the practical rolling-bearing vibration signals. Moreover, the comparison studies are also carried out to show that the proposed method outperforms the traditional basis function expansion methods in weak fault feature extraction of bearing.

1. Introduction

Bearings are widely used in aeroengines. Under severe conditions of high temperature, high pressure, and heavy load, bearings are prone to failures and seriously affect the operational safety of aeroengines [1]. Therefore, it is of great significance to investigate weak-bearing fault features extraction methods in order to detect bearing faults as early as possible and avoid safety accidents.

Many researchers have conducted much research from multiple aspects given the bearing fault diagnosis problem. For the diagnosis problems with massive multivariate data, Yang et al. propose a novel feature extraction method called refined composite multivariate multiscale symbolic dynamic entropy (RCmvMSDE) to extract discriminative and stable features with high efficiency [2]. In order to overcome the difficulties of anomaly detection for multivariate industrial time series such as poor preprocessing efficiency, feature extraction difficulty, and lack of abnormal samples, Liang et al. proposed a novel framework named multitime scale deep convolutional generative adversarial network (MTS-DCGAN) with better model performance and robustness than other comparison algorithms [3]. Besides, variational mode decomposition (VMD) is widely used in bearings fault diagnosis. Zhang et al. proposed a novel method of rolling-bearing fault diagnosis based on VMD and verified that the VMD can accurately extract the principal mode of bearing fault signal, and it better than EMD in bearing defect characteristic extraction [4]. Aiming at the shortcomings of VMD in processing real nonstationary signals, Yan and Jia

proposed a modified method known as cuckoo search algorithm-based variational mode decomposition (CSA-VMD), which decomposes adaptively a multicomponent signal into a superposition of subsignals termed as intrinsic mode function (IMF) by means of parameter optimization [5]. In recent years, intelligent method has also attracted many researchers' attention. Through collocation of clustering methods, such as Euclidean distance (ED) and the kernel method of K-means (KM), Li and Gu developed a set of smart fault-detection approach with chaotic mapping strategy for an industrial ball-bearing system [6]. Zhou et al. proposed a new architecture to recognize the degradation state of the rolling bearing through clustering unlabeled features by k-means and building convolutional neural network recognition model [7]. Instead of preprocessing data, Hoang and Kang use vibration signals directly as input data, proposed a method for diagnosing bearing faults based on a deep structure of convolutional neural network, which has achieved high accuracy and robustness under noisy environments [8].

In actual situations, the original signal collected by the sensor contains a large amount of background noise, and it is challenging to detect accurate bearing state information from it. Thus how to extract fault features under strong noise conditions has become a focused topic since the last several decades [9]. The basis function expansion method represented by wavelet transform has occupied an important position in the fault feature extraction of rotating machinery for a long time [10]. In 1984, French engineer Morlet proposed the wavelet transform with reference to Fourier transform. After years of development, the wavelet theory has included a variety of wavelet basis functions [11]. Babu et al. applied the Daubechies wavelet transform method to the monitoring and diagnosis of rolling bearings [12]. Ma et al. proposed a denoising method based on Morlet wavelet transform and applied it to rolling bearing fault vibration signals [13]. Kumar and Singh proposed a method for measuring the defect width of tapered roller bearing outer ring based on Symlet wavelet decomposition [14]. Once the rolling bearing has a local failure, the shock waveform generated during operation will show unilateral attenuation characteristics. Although the basic functions such as Daubechies wavelet, Morlet wavelet, and Symlet wavelet have localized analysis capabilities, they are all waveforms that oscillate and decay from the middle to the two sides and are not suitable for decomposing unilaterally decayed impulse response signals. According to practical requirements, Lind et al. constructed Laplace wavelet [15], which had received widespread attention because of its unilateral attenuation characteristics similar to the waveform characteristics of bearing fault signals. However, due to the lack of orthogonality, Laplace wavelet cannot directly apply to traditional wavelet transform. Zi et al. proposed the Laplace wavelet correlation filtering method and applied it to the extraction of the impact characteristics of internal combustion engine faults [16].

In recent years, the sparse representation has been drawing increasing attention from researchers since it is an effective and concise signal representation method and can better capture the essential characteristics of the signal [17–21]. The application of basis functions in wavelet transform is restricted, but the sparse representation theory does not have specific requirements for basis functions.

Based on sparse representation theory, various basis functions are applied to the fault diagnosis of rotating machinery. Tang applied the idea of sparse representation to effectively separate the pulse component of the gearbox fault vibration signal based on the Fourier basis function and basis pursuit algorithm [22]. Cai et al. built a dictionary based on the Fourier basis function and short-time Fourier transform by taking the generalized minimax concave (GMC) function as the penalty term, in which the sparse representation coefficients are solved based on the forward-backward splitting (FBS) algorithm. Good results have been achieved in the extraction of transient shock components of gearbox [23]. Aiming at detecting the characteristics of gearbox fault vibration signals, He et al. proposed a signal sparse representation method based on the adjustable Q-factor wavelet and augmented Lagrangian multiplier method to separate transient shock components and harmonic components from gearbox fault vibration signals [24].

In the practical applications, the type of basis function will directly affect the sparsity of the sparse representation of the signal. Therefore, the choice of basis function needs to conform to the waveform characteristics of the signal transient impulse component as much as possible. Fourier basis and adjustable Q factor wavelet basis can be successfully applied to gearboxes. Still, they are not suitable for extracting unilateral attenuation waveforms from the vibration signals of the bearing fault. Furthermore, the algorithms such as basis pursuit, forward-backward splitting, and augmented Lagrangian multipliers have the problems of high computational complexity and slow convergence speed [25, 26].

The motivation of this paper is to detect a weak-bearing fault feature extraction method under the framework of sparse representation. The Laplace wavelet is used to select the sparse dictionary and obtain the sparse representation of the vibration signals since it is similar to the impact waveform of the bearing fault signal. In addition, the orthogonal matching pursuit algorithm is used to obtain the coefficients of the sparse representation, which takes advantage of the small amount of calculation, high computational efficiency, and strong feasibility [27]. Simulation examples and experimental examples examine the proposed method. The comparisons of the proposed method with the traditional basis function expansion method are also carried out to show the applicability and effectiveness of the proposed method.

2. Sparse Representation of Signal Transient Impact Components

2.1. Principle of Sparse Representation. Sparse representation is to express an arbitrarily complex signal as a linear superposition form of the optimal basic waveform matching the structural characteristics of the signal through an

appropriate overcomplete redundant dictionary, using as few atoms as possible [28]. A dictionary is a collection of generalized basis functions, including a series of parameterized or nonparameterized basic waveforms. A single basic waveform in the dictionary is called an atom. Atom is the basic unit of signal sparse representation and contains information about the signal. The atom herein is different from the basis function in the traditional method. The traditional signal analysis method is mainly based on the basis function expansion. The basis function must strictly satisfy orthogonality, and the types of the basis functions are limited. However, the atoms have no orthogonality constraints, any form of waveform structure can be introduced to represent the original signal, which means that multiple atoms can represent each other. This property is called redundancy. Moreover, there is no limit to the number of atoms in a dictionary, and it can even be greater than the length of signal, which means it is overcomplete.

In mathematics, the original signal x can be represented by a series of column vectors. The dictionary Φ is composed of M column vectors, and each column vector is an atom φ_k ($k \in (1, M)$). Select several suitable atoms from the overcomplete redundant dictionary to sparsely represent the original signal. This process can be expressed as

$$x = \hat{x} + x_r = \sum_{k=1}^{M} \alpha_k \varphi_k + x_r, \tag{1}$$

where $\hat{x}$ is the approximation signal of the original signal $x \in R^N$, x_r is the residual term, and α_k is the sparse representation coefficient corresponding to the kth atom φ_k.

The essence of sparse representation is an optimization problem, and it is hoped that the sparse representation result of the original signal x can be obtained when the residual term x_r is small enough. Then the sparse representation model can be constructed as follows:

$$\begin{aligned} &\min \quad \|\alpha\|_0 \\ &\text{s.t.} \quad \|x - \Phi\alpha\|_2^2 \le \varepsilon, \end{aligned} \tag{2}$$

where $\alpha = [\alpha_1, \alpha_2, \ldots, \alpha_M] \in R^{M\times 1}$ is the sparse representation coefficient matrix, $\Phi = [\varphi_1, \varphi_2, \ldots, \varphi_K] \in R^{N\times K}\,(K > N)$ is the constructed overcomplete redundancy dictionary, the objective function of the above model is represented by the l_0-norm $\|\alpha\|_0$ of the sparse representation coefficient matrix α, and the l_0-norm represents the number of nonzero elements in the matrix, which is also called the sparsity of the coefficient matrix.

This optimization problem is a typical NP-hard problem [29, 30]. The amount of calculation to solve the optimal solution is too large, and it can only accept suboptimal solutions that are sparse enough. For this reason, researchers have proposed a variety of algorithms such as matching pursuit, basis tracking, and orthogonal matching pursuit. It can be seen from the above model that two problems need to be solved to achieve the sparse representation of the signal: (1) How to construct an appropriate overcomplete redundant dictionary Φ and (2) How to solve the suboptimal sparse representation coefficient matrix α. These two problems can be solved by the dictionary construction method and the atomic decomposition algorithm. The signal sparse representation process is shown in Figure 1.

2.2. Laplace Wavelet Correlation Filtering Method. The Laplace wavelet is a typical nonorthogonal complex exponential wavelet with apparent unilateral attenuation characteristics. The wavelet decays in a "spiral shape" in the complex space. As shown in Figure 2, both the real number form and the imaginary number form are very similar to the unilateral attenuation curve of a single degree of freedom structure. Since the rolling bearing vibration signal is an actual signal, only the real number form of Laplace wavelet is considered, and its analytical expression is as follows:

$$\begin{aligned} \varphi(\tau, t) = \psi_\gamma(t) &= \psi(f, \zeta, \tau, t), \\ &= \begin{cases} Ae^{-\zeta/\sqrt{1-\zeta^2}\,2\pi f(t-\tau)} \sin(2\pi f(t-\tau)), & t \in [\tau, \tau + Ws], \\ 0, & \text{others}, \end{cases} \end{aligned} \tag{3}$$

where $f \in R^+$ represents the oscillation frequency, $\zeta \in [0, 1)$ represents the viscous damping ratio, the larger ζ is the faster the Laplace wavelet waveform attenuates, $\tau \in R$ represents time parameter, coefficient A is used to achieve amplitude normalization, $Ws \in R^+$ indicates the width of time support, and parameter vector $\gamma = (f, \zeta, \tau)$ determines the wavelet structure and the information contained in the wavelet.

Suppose three vectors F, Z, T correspond to the discretization parameters f, ζ, τ, respectively, which can be expressed as

$$\begin{aligned} F &= \{f_1, f_2, \ldots, f_m\} \subset R^+, \\ Z &= \{\zeta_1, \zeta_2, \ldots, \zeta_n\} \subset [0, 1), \\ T &= \{\tau_1, \tau_2, \ldots, \tau_p\} \subset R. \end{aligned} \tag{4}$$

Then the Laplace wavelet basic waveform library can be defined as a set Ψ of a group of waveforms $\psi_\gamma(t)$, which can be expressed as $\Psi = \{\psi(f, \zeta, \tau, t):\ f \in F, \zeta \in Z, \tau \in T\}$.

The correlation coefficient can evaluate the similarity of two sets of signals, which can be defined by the inner product. For two discrete vectors x, y of finite length, the inner product is expressed as

$$\langle x, y\rangle = \|x\|_2 \|y\|_2 \cos\theta, \tag{5}$$

where θ is related to the linearity between x and y, which can reflect the relativity of the two vectors. If x and y are completely linearly related, then A is θ equal to 0. Define the correlation coefficient cc as $\cos\theta$, which holds

$$cc = \cos\theta = \frac{|\langle x, y\rangle|}{\|x\|_2 \|y\|_2}. \tag{6}$$

The correlation coefficient reflects the degree of correlation between x and y. If x and y are completely linearly related, then $cc = 1$.

The correlation filtering method [31] uses the basic waveform parameters τ of different Laplace wavelets in the basic waveform library to achieve translation across the

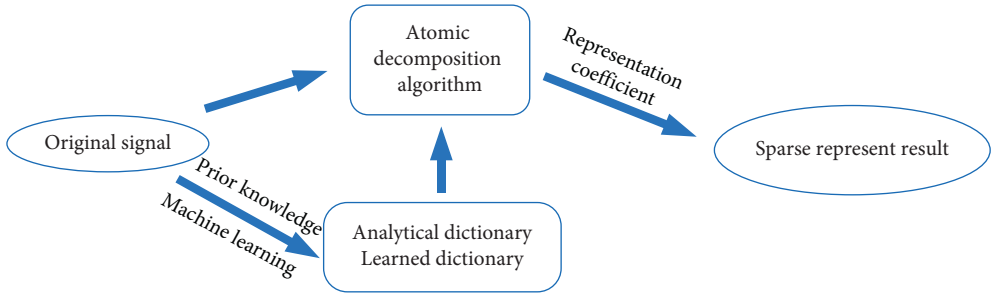

Figure 1: Signal sparse representation process.

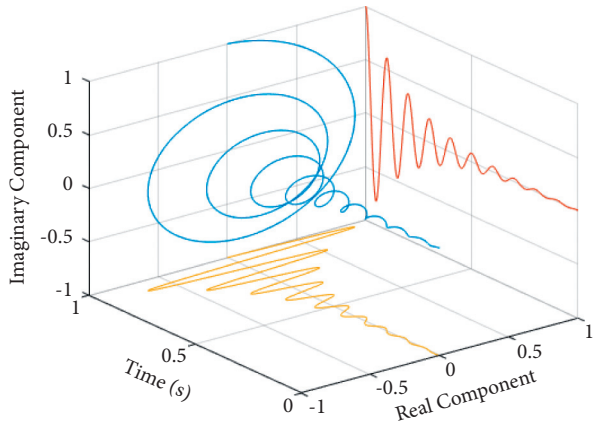

Figure 2: Laplace wavelet waveform.

entire time history of the signal. It calculates the correlation coefficient between each wavelet atom and the signal. The maximum correlation coefficient value indicates that the modal parameter of the measured object at the moment $(\overline{\tau})$ is closest to the parameter $(\overline{f}, \overline{\zeta})$ corresponding to the basic waveform of the Laplace wavelet.

The basic waveform above is called the optimal Laplace wavelet atom. The correlation filtering method cannot directly construct an analytical dictionary but can only find a wavelet atom most similar to the original signal transient impulse waveform structure. To construct the dictionary, the sparseness and periodicity of the impact component in the rolling bearing fault signal can expand the optimal wavelet atom $\psi(\overline{f}, \overline{\zeta})$ into a series of wavelet atoms by changing the time parameter τ, thus forming the Laplace wavelet dictionary $\Phi(\overline{f}, \overline{\zeta}, \tau, t)$. Then, to ensure the accuracy of the sparse representation result, the translation step of the time parameter τ takes the inverse of the sampling frequency.

2.3. Orthogonal Matching Pursuit Algorithm. The orthogonal matching pursuit (OMP) algorithm is a typical greedy algorithm developed from the matching pursuit (MP) algorithm. Orthogonal matching pursuit is essentially an iterative decomposition process. First, according to the correlation, select the atom that best matches the current residual signal structure feature in the overcomplete redundant dictionary. Then, perform Schmidt orthogonalization on all the selected atoms, remove the component corresponding to the atom from the signal, and obtain the residual signal of the next iteration. The residuals are orthogonal to the selected atoms in each iteration. Finally, iterate until the residual signal reaches a certain approximation accuracy or reaches a predetermined number of iterations. Then, the signal can be approximated by a linear combination of multiple atoms.

To solve the problem of slow convergence speed and the large number of iterations of the MP algorithm, the OMP algorithm adds an orthogonalization process in each iteration process to ensure that the residual signal is orthogonal to all selected atoms. In the ith iteration, define a matrix Φ_1 and subspace V composed of all the selected atoms $\varphi_{\gamma 1}, \varphi_{\gamma 2}, \ldots, \varphi_{\gamma i}$, and then the operator of orthogonal projection to the subspace V is $\Phi_1(\Phi_1^T\Phi_1)^{-1}\Phi_1^T$. The iterative update of the residual term can be expressed as

$$r_{i+1} = r_i - \Phi_1\left(\Phi_1^T\Phi_1\right)^{-1}\Phi_1^T r_i. \tag{7}$$

For the known original signal x and dictionary Φ, the specific process of orthogonal matching pursuit is as follows.

(1) Initialization: suppose the residual term is r_0, set the iteration decomposition number $i = 1$, and give the iteration termination condition, which is the signal approximation accuracy requirement ε or the maximum iteration decomposition number n.

(2) Optimization problem. Solve

$$\max_{\varphi_\gamma} \langle r_{i-1}, \varphi_\gamma \rangle. \tag{8}$$

Calculate the inner product of r_{i-1} and each atom $\varphi(\tau, t)$ in the dictionary Φ, the atom with the largest inner product is the optimal atom $\varphi_{\gamma i}$ for this iteration. The essence of this step is to solve the optimization problem of Formula (2).

(3) Update. Calculate the weighting factor

$$\alpha_i = \langle r_{i-1}, \varphi_{\gamma i} \rangle. \tag{9}$$

Update residual items. Define a matrix Φ_1 composed of all selected atoms $\varphi_{\gamma 1}, \varphi_{\gamma 2}, \ldots, \varphi_{\gamma i}$, the iterative update of the residual items can be expressed as

$$r_{i+1} = r_i - \Phi_1\left(\Phi_1^T\Phi_1\right)^{-1}\Phi_1^T r_i, \tag{10}$$

where $\Phi_1(\Phi_1^T\Phi_1)^{-1}\Phi_1^T$ is an orthogonal operator.

(4) Judge the termination condition of iteration by

$$\frac{\|r_i\|_2}{\|x\|_2} \leq \varepsilon, \text{or}, i = n. \tag{11}$$

The orthogonal matching pursuit is terminated if the iteration termination condition is met. If the termination conditions are not met, continue to set $i = i + 1$, and perform steps (2)~(4) again.

(5) Output iteration results. Reconstructed signal $\hat{x}$ by

$$\hat{x} = \sum_{i=1}^{n} \alpha_i \varphi_{\gamma i}. \tag{12}$$

2.4. Computation Complexity. As described in 2.2 and 2.3, this method has parameters such as F, Z, n, and x. The computation complexity (FLOPs) under different parameters is shown in Table 1. First, it can be seen from Table 1 that the sequence length of x can significantly affect the performance of this method, the computation complexity increases by the square of the sequence length of x. Besides, the number of iterations is closely related to the algorithm performance, and the computation complexity is proportional to n. Compared with x and n, remaining parameters such as Ws, F, and Z have much less effect on the algorithm performance. The increment of computation complexity is proportional to the number of F, the number of Z, and the length of Ws.

Table 1: The computational complexity (FLOPs) under different parameters.

Length of x	Length of Ws	Number of F	Number of Z	n	FLOPs
1000	25	2	2	10	21.76M
1000	25	2	2	20	43.50M
1000	25	2	2	40	89.44M
1000	25	4	2	10	22.27M
1000	25	8	2	10	23.31M
1000	25	4	4	10	23.31M
1000	25	2	4	10	22.28M
1000	25	2	8	10	23.31M
1000	50	2	2	10	23.10M
1000	100	2	2	10	25.78M
2000	25	2	2	40	338.73M
4000	100	8	8	10	463.79M
4000	25	2	2	40	1317.29M

3. Analysis of Simulation Examples

To verify the applicability of extracting the weak impact component of the signal through orthogonal matching pursuit under the Laplace wavelet dictionary, a cyclic unilateral attenuation impact signal is constructed below, and the simulation signal is analyzed. The signal is composed of the Laplace wavelet base and Gaussian white noise. The Laplace wavelet simulates the impact component in the fault vibration signal of rotating machinery, and the background noise is affected by Gaussian white noise. The simulation signal expression is as follows:

$$\begin{aligned} x(t) &= \sum_i \mathrm{d}(t - iT_0) + A_n n(t) \\ &= \sum_i \left[e^{-\zeta_0/\sqrt{1-\zeta_0^2}\cdot 2\pi f_0 (t-\tau_0-iT_0)} \times \sin 2\pi f_0 (t - \tau_0 - iT_0) \right] \\ &\quad + A_n n(t). \end{aligned} \tag{13}$$

where time $t \in [0, 1]$, oscillation frequency $f_0 = 200$ Hz, viscous damping ratio $\zeta_0 = 0.05$, $\tau_0 = 0.1$ s, transient shock cycle $T_0 = 0.2$ s, number of cycles $i = 0, 1, 2, 3, 4$, noise amplitude $A_n = 0.1$ m/s^2, $n(t)$ is Gaussian white noise with a noise intensity of 0.2 dBw, signal-to-noise ratio after adding noise to the signal is −10.458 dB, and the sampling frequency for discretizing the signal is 2000 Hz. The simulation signal is shown in Figure 3. Figure 3(a) is the time-domain waveform of the cyclic unilateral attenuation simulation signal, and Figure 3(b) is the simulation signal after adding noise.

According to the correlation filtering method, it is calculated that the maximum value of the correlation coefficient is obtained at time $\overline{\tau} = 0.1$ s, and the Laplace wavelet atom that best matches the original signal is obtained. The maximum value of the correlation coefficient is 0.821, and the optimal wavelet atom can be expressed as $\overline{d}(t, \overline{\tau}) = \psi_1(\overline{f}, \overline{\zeta}, \overline{\tau}, t)$, where $\overline{f} = 197$ Hz, $\overline{\zeta} = 0.045$, $\overline{\tau} = 0.3$ s. The optimal wavelet atom is shown in Figure 4(a). Keeping the oscillation frequency $\overline{f}$ and viscous damping ratio $\overline{\zeta}$ unchanged, τ is equally spaced in the entire time history according to the reciprocal of the sampling frequency $(1/f_s)$, and a redundant Laplace wavelet dictionary $D(\tau, t) = \psi(197, 0.045, \tau, t)$ is obtained. The sparse representation coefficients can be obtained by solving the model with the OMP algorithm, as shown in Figure 4(b), where the signal approximation accuracy is required to be 0.1. The relatively large nonzero coefficients in the figure appear at 0.1, 0.3, 0.5, 0.7, and 0.9 s, respectively, corresponding to the moment when the transient impact component of the simulation signal is generated. Figure 4(c) shows the signal waveform obtained from sparse representation sparse reconstruction. Perform Hilbert envelope demodulation analysis on the reconstructed signal in Figure 5 to get the envelope spectrum, as shown in Figure 6. The characteristic frequency of the reconstructed signal is 5 Hz, which is consistent with the theoretical value.

The correlation coefficient can reflect the similarity of the two signals. The correlation coefficient is calculated on the reconstructed signal in Figure 7 and the noise-free simulation signal in Figure 3(a). The correlation coefficient is 0.821, which shows that the method in this paper can accurately determine the moment when the transient impact component is generated for the cyclic unilateral attenuation signal. The extracted impact component is also very similar to the unilateral attenuation waveform in the simulation signal.

To further verify the method's ability to identify the moment of transient impact components and its anti-interference ability against strong noise, Table 1 lists the identified impact response moments under different noise intensities and gives the correlation coefficients of the corresponding reconstructed signal and the original noise-

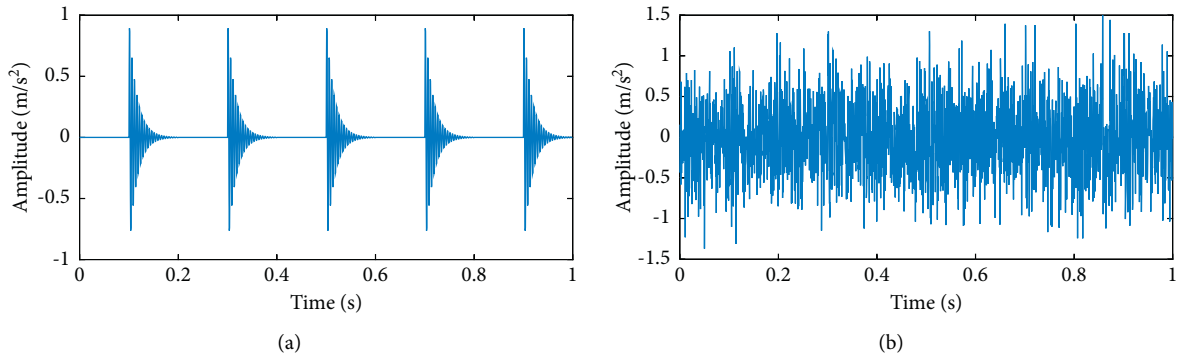

Figure 3: The simulation signal. (a) Cyclic unilateral attenuation simulation signal. (b) The noisy simulation signal.

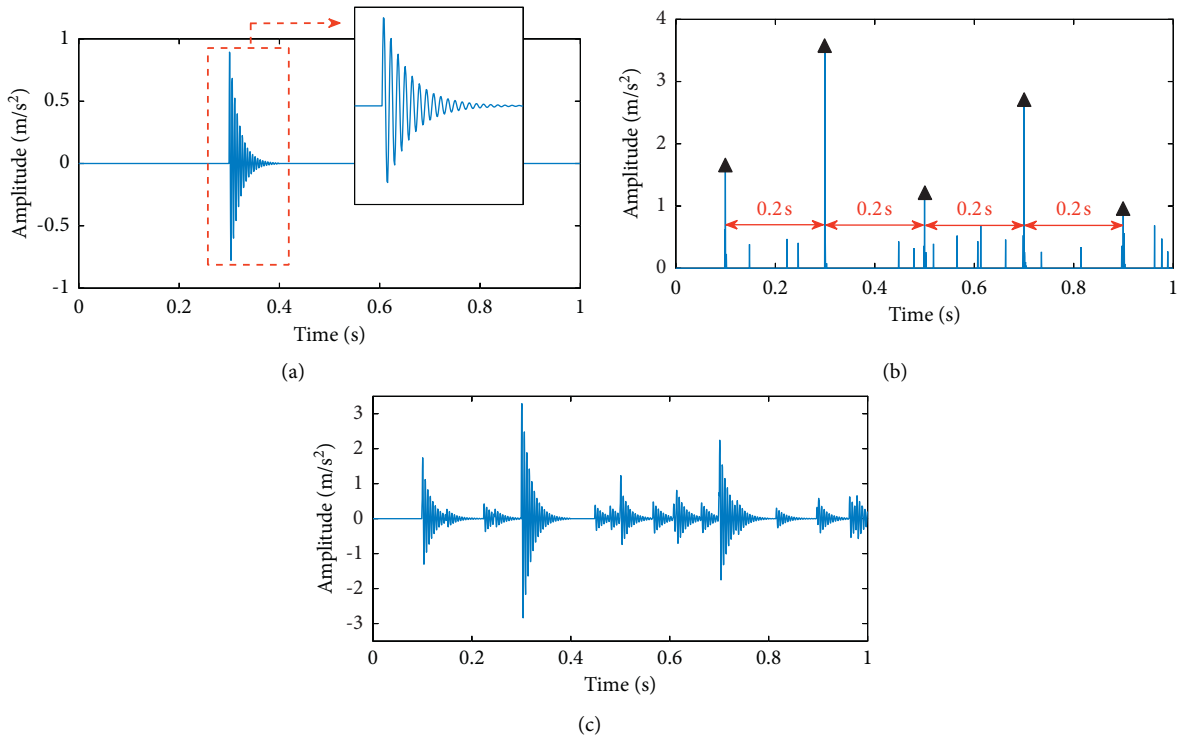

Figure 4: Results of sparse representation. (a) The optimal Laplace wavelet atom. (b) Sparse representation coefficient. (c) The reconstructed signal.

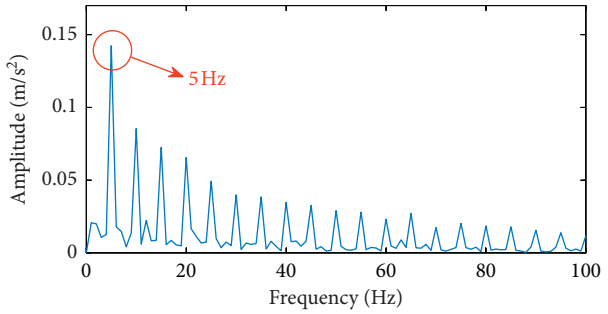

Figure 5: The envelope spectrum for the reconstructed signal.

free signal. In the table, P_n represents the noise intensity, SNR represents the signal-to-noise ratio, t_i represents the impulse response time identified by this method, and CC represents the correlation coefficient of the reconstructed signal and the original no-noise signal. The signal-to-noise ratio is defined as $\mathrm{SNR} = 10 \times \lg(P_s/P_n)$, where P_s and P_n represent the intensity of the noise-free signal and noise, respectively.

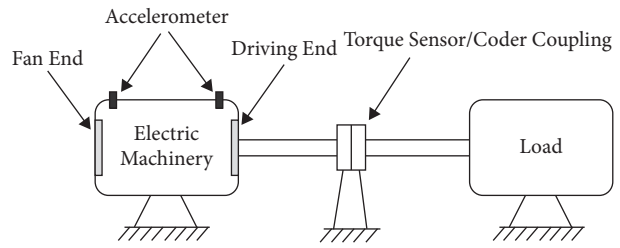

Figure 6: Schematic diagram of the experimental rig.

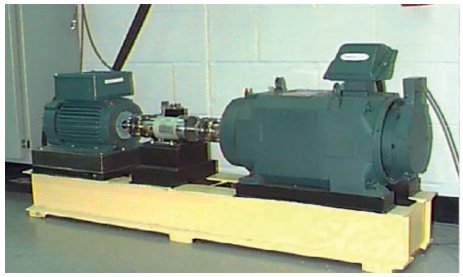

Figure 7: Experiment rig of the rolling bearing.

It can be seen from Table 1 that when the signal-to-noise ratio reaches −17.447, the difference between the identified impulse response time and the impulse response time of the original signal is still slight. In contrast, the correlation coefficient of the reconstructed signal and the original signal is not low. As the signal-to-noise ratio increases, the correlation coefficient of the reconstructed signal and the original no-noise signal rises rapidly, and the effect of signal reconstruction has also become better. It can accurately identify when the impulse response occurs and better restore the original signal.

4. Analysis of Experimental Examples

To further verify the effectiveness of the Laplace wavelet combined with orthogonal matching pursuit in extracting weak fault characteristics of bearings, the proposed method is applied to extract the transient impact components of the fault vibration signals of the inner and outer rings of rolling bearings. Because the contact between the rolling element and the fault point of the inner/outer ring is intermittent and cyclic in time at a constant speed, the shock component of the vibration signal appears as a sparse and periodic unilateral attenuation waveform. Then sparse representation can be achieved by the method proposed in this paper.

The experimental calculation examples in this paper quoted the rolling bearing vibration acceleration signal from the Bearing Data Center of Western Reserve University in the United States [32, 33]. These data are widely used in the research of fault diagnosis of rotating machinery. The appearance of the experimental platform is shown in Figure 7, and the schematic diagram is shown in Figure 6. The experimental platform consists of four parts, including a 1.5KW motor, torque sensor, power tester, and electronic controller (not included in the picture). The tested bearing is installed above the bearing seat of the fan end and the drive end of the motor. The motor shaft is supported by the bearing to be tested and provides power for the bearing. The bearing model of the fan end is SKF6203-2RS, and the bearing model of the drive end is SKF6205-2RS. A 16-channel data collector collects the acceleration signal, and the sampling frequency is 12 k and 24 k. The pitting failures were processed in the rolling element, inner ring, and outer ring using the electric discharge machine. The fault diameter includes 0.1778, 0.3556, and 0.5334 mm and the fault depth is 0.2794 mm. Working conditions include four speeds of 1730, 1750, 1772, and 1797 rpm and four loads of 0, 0.75, 1.5, and 2.25 kW. The experiment collects a set of experimental data with a length of 120,000 under different loads, different speeds, and different levels of failure.

The lengthy experimental data were screened to study the extraction of weak fault features, and the rolling bearing model SKF6205-2RS was selected as the research object. The data came from the driving end. The structural parameters of the bearing are shown in Table 2 [33]. A pitting failure with a diameter of 0.1778 mm and a depth of 0.2794 mm was machined using the electric discharge machine to simulate the local weak failure of the bearing in engineering applications. The spindle speed is 1730 rpm ($f_r = 28.83$ Hz), the sampling frequency is 12 kHz, the load is 0, the number of sampling points is 2400, and the sampling time $t = 0.2$ s. After calculation, the theoretical values of the fault characteristic frequencies corresponding to the inner ring and the outer ring are 156.14 Hz and 103.36 Hz.

4.1. Feature Extraction of Weak Faults in Bearing Inner Ring. The time-domain waveform of the weak fault vibration signal of the inner ring of the rolling bearing is shown in Figure 8. The time-domain waveform is used as the research object for extracting the weak fault feature of the inner ring based on the Laplace wavelet combined with orthogonal matching pursuit.

First, perform correlation filtering calculations on the waveform shown in Figure 8 to obtain the Laplace wavelet atom that best matches the time domain waveform. The optimal wavelet atom can be expressed as $d(t, \overline{\tau}) = \psi_1(\overline{f}, \overline{\zeta}, \overline{\tau}, t)$, where $\overline{f} = 3610$ Hz, $\overline{\zeta} = 0.03$, and $\overline{\tau} = 0.0638$ s. The optimal wavelet atom is shown in Figure 9(a). Keeping the oscillation frequency $\overline{f}$ and viscous damping ratio $\overline{\zeta}$ unchanged, τ is equally spaced in the entire time history according to the reciprocal of the sampling frequency $(1/f_s)$, and a Laplace wavelet dictionary $D(\tau, t) = \psi(3610, 0.03, \tau, t)$ is obtained.

Second, the sparse representation coefficient is solved by the orthogonal matching pursuit algorithm, and the signal approximation accuracy is set to 0.1. The calculation result is shown in Figure 9(b). From the figure, the time when the impact component of the inner ring fault is generated can be intuitively distinguished. Figure 9(c) shows the weak fault vibration signal of the bearing inner ring reconstructed from the Laplace wavelet dictionary and the sparse representation coefficient.

Perform Hilbert envelope demodulation on the reconstructed signal to get its envelope spectrum, as shown in Figure 10. It shows that the characteristic frequency of the inner ring impact fault of the rolling bearing is 155.5 Hz, which is basically consistent with the theoretical value. It can be seen that the method proposed in this paper can effectively extract the characteristic frequency of the inner ring impact fault under strong noise.

4.2. Feature Extraction of Weak Faults in Bearing Outer Ring. The time-domain waveform of the weak fault vibration signal of the outer ring of the rolling bearing is shown in Figure 11. The time-domain waveform is used as the

Table 2: The analysis results the simulated signal with the proposed method at different SNR.

$P_n/dB\ w$	SNR/dB			t_i/s			CC
0.03	−2.218	0.100	0.300	0.500	0.700	0.900	0.969
0.04	−3.347	0.100	0.300	0.500	0.700	0.900	0.945
0.06	−5.229	0.100	0.300	0.500	0.700	0.900	0.944
0.08	−6.478	0.100	0.300	0.500	0.700	0.900	0.916
0.1	−7.447	0.097	0.300	0.499	0.700	0.897	0.876
0.15	−9.208	0.100	0.300	0.500	0.700	0.900	0.861
0.2	−10.458	0.100	0.300	0.500	0.700	0.900	0.821
0.3	−12.218	0.099	0.301	0.497	0.699	0.899	0.771
0.5	−14.437	0.100	0.297	0.500	0.695	0.891	0.686
1	−17.447	0.099	0.283	0.500	0.692	0.898	0.582

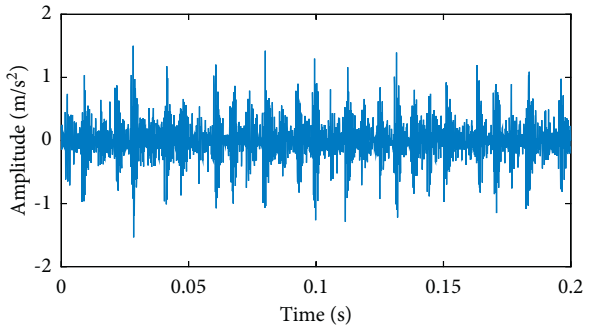

Figure 8: Time-domain waveform of impact fault of bearing inner ring.

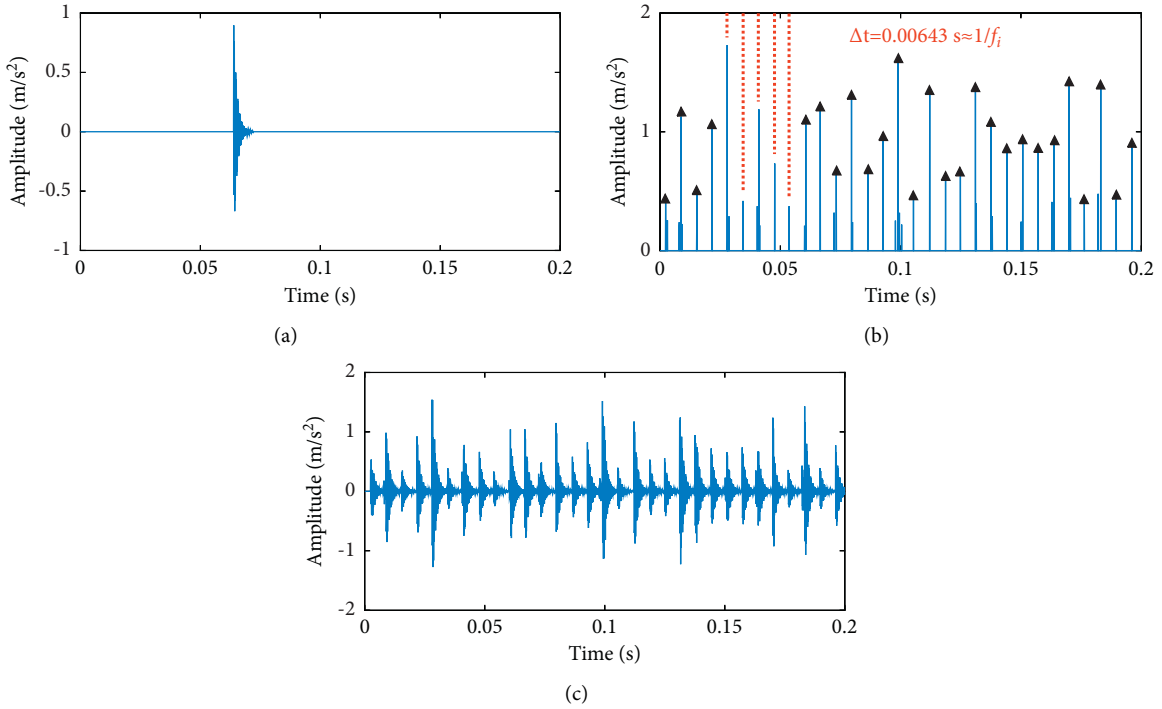

Figure 9: The results of sparse representation of the vibration signal of the weak fault of the bearing inner ring. (a) The optimal Laplace wavelet atom. (b) Sparse representation coefficients. (c) The reconstructed signal.

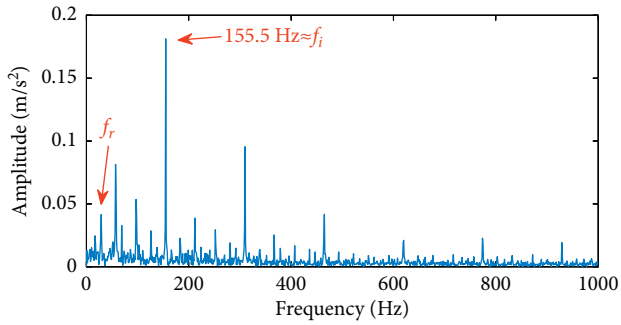

Figure 10: The envelope spectrum for the reconstructed signal of inner ring fault.

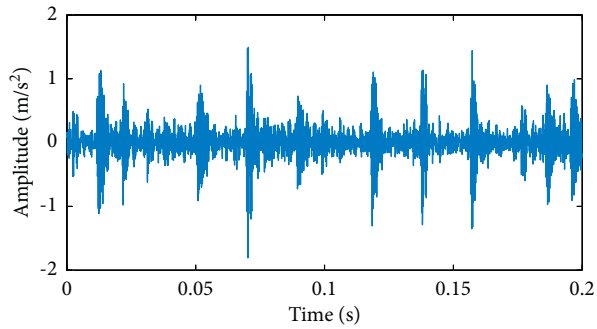

Figure 11: Time-domain waveform of weak fault vibration signal of bearing outer ring.

research object for extracting the weak fault feature of the outer ring based on Laplace wavelet combined with orthogonal matching pursuit.

First, perform correlation filtering calculations on the waveform shown in Figure 11 to obtain the Laplace wavelet atom that best matches the time domain waveform. The optimal wavelet atom can be expressed as $\overline{d}(t, \overline{\tau}) = \psi_1(\overline{f}, \overline{\zeta}, \overline{\tau}, t)$, where $\overline{f} = 3390$ Hz, $\overline{\zeta} = 0.01$, and $\overline{\tau} = 0.1571$ s. The optimal wavelet atom is shown in Figure 12(a). Expand the Laplace wavelet dictionary $D(\tau, t) = \psi(3390, 0.01, \tau, t)$ from the optimal wavelet atom.

Second, the sparse representation coefficient is solved by the orthogonal matching pursuit algorithm, and the signal approximation accuracy is set to 0.1. The calculation result is shown in Figure 12(b). From the figure, it is possible to visually distinguish the time when the outer ring fault impact component occurs. Figure 12(c) shows the reconstructed vibration signal of the weak fault of the bearing outer ring.

Perform Hilbert envelope demodulation on the reconstructed signal to get its envelope spectrum, as shown in Figure 13. It shows that the characteristic frequency of the outer ring impact fault of the rolling bearing is 103.2 Hz, which is basically consistent with the theoretical value. It can be seen that the method proposed in this paper can effectively extract the characteristic frequency of the outer ring impact fault under strong noise.

4.3. Feature Extraction Results of Weak-Bearing Faults. The above-mentioned experimental analysis shows that the characteristic frequencies of the bearing inner ring fault and outer ring fault extracted by the method proposed in this paper are basically consistent with the theoretical values, and the relative errors are 0.730% and 0.832%, respectively. The method proposed in this paper can effectively extract the weak fault characteristics of the bearing under strong background noise.

To further verify the superiority of the proposed method compared with the traditional basis function expansion method, a comparative analysis of the amplitude of the fault characteristic frequency extracted by various methods is carried out. The wavelet transform method used in literature [14–16] is selected as the control group, and Symlet wavelet base, Morlet wavelet base, and Daubechies base are used, respectively. In order to enhance the reliability of the calculation results, calculate 20 vibration signals with a length of 0.2 s and take the average value as the calculation result. Comparing the extraction effects of several methods is essentially comparing the prominence of the characteristic frequency in the frequency spectrum. Therefore, it is necessary to set a dimensionless characteristic quantity as an evaluation index. The frequency conversion amplitude is taken as the benchmark to normalize the amplitude, and the calculate results are shown in Table 3. We can observe that the normalized amplitude of the inner ring impact fault extracted based on the method proposed in this paper is 9.68%–20.45% better than the wavelet transform. The extracted outer ring impact fault characteristic frequency normalized amplitude is 18.49%–68.27% better than wavelet transform. It means that the fault characteristic frequency obtained by the method proposed in this paper is more prominent, which is helpful to identify the fault

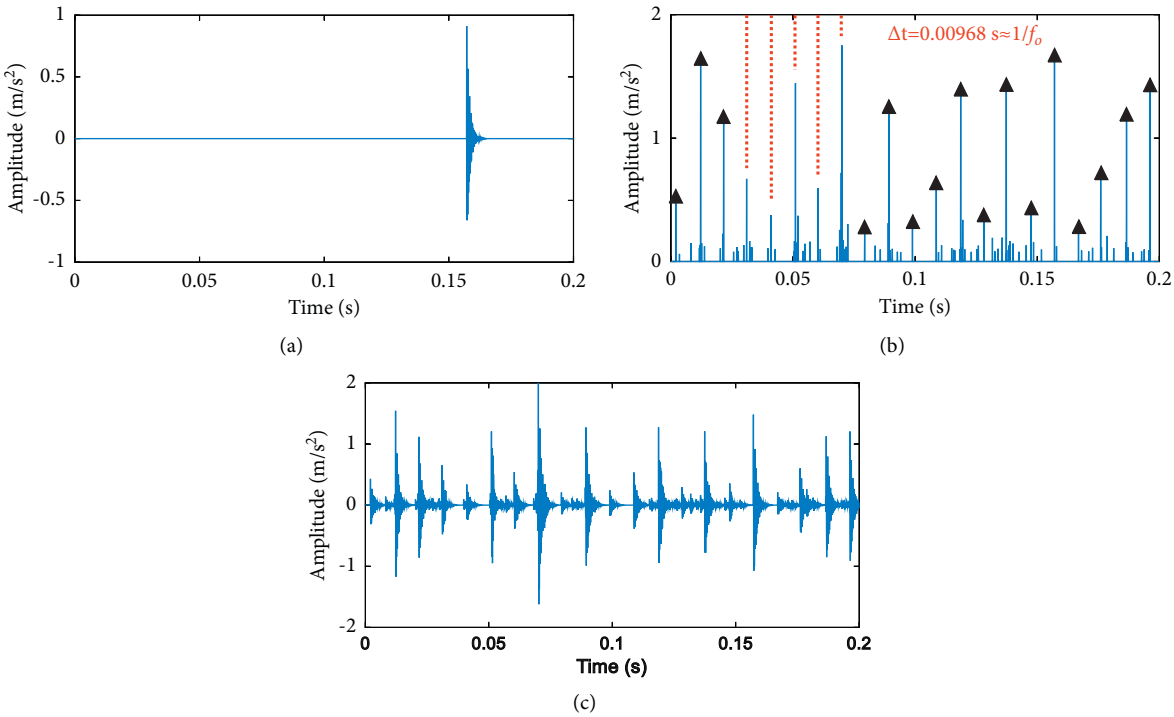

Figure 12: The results of sparse representation of the vibration signal of the weak failure of the outer ring of the bearing. (a) The optimal Laplace wavelet atom. (b) Sparse representation coefficients. (c) The reconstructed signal.

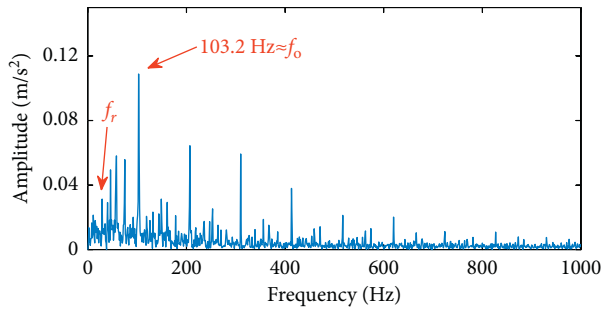

Figure 13: The envelope spectrum for the reconstructed signal of outer ring fault.

Table 3: Parameters of deep groove ball-bearing SKF6205-2RS.

Parameter name	Parameter value
Number of rolling elements	9
Inner ring diameter (mm)	25
Outer ring diameter (mm)	52
Pitch diameter (mm)	39.04
Rolling element diameter (mm)	7.94
Contact angle (°)	0
Inner ring impact fault characteristic frequency f_i (Hz)	156.14
Outer ring impact fault characteristic frequency f_o (Hz)	103.36

type of the bearing. In summary, from the perspective of the frequency and amplitude of the fault, the method proposed in this paper has more significant advantages than the traditional basis function expansion method represented by wavelet transform and has achieved good results in bearing fault diagnosis, as shown in Table 4.

Table 4: Normalized amplitude of fault characteristic frequency.

	Normalized amplitude of inner ring impact fault	Normalized amplitude of outer ring impact fault
Daubechies wavelet transform	3.622	2.931
Morle wavelet transform	3.692	2.455
Symlet wavelet transform	3.979	2.064
Laplace wavelet and orthogonal matching pursuit	4.364	3.473

5. Conclusions

Under the framework of sparse representation theory, a feature extraction method for weak-bearing faults based on Laplace wavelet and orthogonal matching tracking is proposed. It mainly solves two problems in the sparse representation of signals:

On the one hand, the optimal wavelet atom is obtained through the Laplace wavelet correlation filtering method, and the time parameters are changed to expand into a wavelet dictionary; on the other hand, the orthogonal matching pursuit algorithm is used to solve the sparse representation coefficients, and the transient impact components in the vibration signal are converted into a series of representation coefficients under the wavelet dictionary. Aiming at the sparse representation of the signal, the Hilbert resonance demodulation method is used to obtain the fault characteristic frequency, and the weak fault characteristic extraction under strong background noise is realized.

Through the analysis of simulation examples, it is found that the proposed method can identify the moment when the transient impact component is generated, and the anti-interference ability against strong noise is verified. These results show that the method in this paper is suitable for extracting the weak impact component under strong noise. Then, the proposed method is applied to the feature extraction of rolling bearing faults. The analysis results show that the method can effectively extract the characteristic frequencies of weak inner ring faults and weak outer ring faults and then accurately judge the state of the bearing. The three wavelet transform methods mentioned in literature 3–5 are used to extract the characteristic frequency amplitude of the bearing fault, and the characteristic frequency amplitude of the fault is processed nondimensionally based on the rotation frequency amplitude. The comparison and analysis of the feature extraction effect of the method in this paper and the three wavelet transform methods verify the superiority of the method in this paper compared with the traditional basis function expansion method.

Nomenclature

x: Original signal
$\hat{x}$: Approximation signal
x_r: Residual term
Φ, D: Dictionary
φ_k: Atom
α: Sparse representation coefficient matrix
α_k: Sparse representation coefficient
f: Oscillation frequency
ζ: Viscous damping ratio
τ: Time parameter
t: Time
A: Amplitude coefficient
Ws: Width of time support
n: Number of iterations of OMP algorithm
r_i: i th iteration
cc: CC correlation coefficient
P_s: Noise-free signal intensity
P_n: Noise intensity
SNR: Signal-to-noise ratio.

Data Availability

The data sets generated during and/or analyzed during the current study are available from the corresponding author on reasonable request.

Conflicts of Interest

The authors declare that they have no conflicts of interest.

Acknowledgments

The authors are very grateful for the financial supports from the National Major Science and Technology Projects of China (Grant no. 2017-IV-0008-0045), the National Natural Science Foundation of China (Grant nos. 11972129 and 12172307), Department of Science & technology of Liaoning province (Grant no. 2019BS182), the Educational Department of Liaoning province (Grant no. LJGD2019009), and the Opening Project of Applied Mechanics and Structure Safety Key Laboratory of Sichuan Province (Grant no. SZDKF-201903).

References

[1] N. Sawalhi and R. B. Randall, "Simulating gear and bearing interactions in the presence of faults," *Mechanical Systems and Signal Processing*, vol. 22, no. 8, pp. 1924–1951, 2008.

[2] Y. T. Yang, H. L. Zheng, J. C. Yin, M. Xu, and Y. Chen, "Refined composite multivariate multiscale symbolic dynamic entropy and its application to fault diagnosis of rotating machine," *Measurement*, vol. 151, Article ID 107233, 2020.

[3] H. Liang, L. Song, J. Wang, L. Guo, X. Li, and J. Liang, "Robust unsupervised anomaly detection via multi-time scale DCGANs with forgetting mechanism for industrial multivariate time series," *Neurocomputing*, vol. 423, pp. 444–462, 2021.

[4] M. Zhang, Z. Jiang, and K. Feng, "Research on variational mode decomposition in rolling bearings fault diagnosis of the multistage centrifugal pump," *Mechanical Systems and Signal Processing*, vol. 93, pp. 460–493, 2017.

[5] X. Yan and M. Jia, "Application of CSA-VMD and optimal scale morphological slice bispectrum in enhancing outer race fault detection of rolling element bearings," *Mechanical Systems and Signal Processing*, vol. 122, pp. 56–86, 2019.

[6] S. Y. Li and K. R. Gu, "smart fault-detection machine for ball-bearing system with chaotic mapping strategy," *Sensors*, vol. 19, no. 9, 2019.

[7] Q. C. Zhou, H. H. Shen, J. Zhao, X. Liu, and X. Xiong, "Degradation state recognition of rolling bearing based on K-means and CNN algorithm," *Shock and Vibration*, vol. 20199 pages, Article ID 8471732, 2019.

[8] D. T. Haong and H. J. Kang, "Rolling element bearing fault diagnosis using convolutional neural network and vibration image," *Cognitive Systems Research*, vol. 53, pp. 42–50, 2019.

[9] G. Dong, J. Chen, and H. Yuan, "Study on feature extraction of bearing incipient weak fault based on dictionaryrn learning," *Condition Monitoring & Diagnostic Engineering Management*, vol. 21, no. 3, pp. 9–14, 2018.

[10] Z. Feng, X. Chen, and M. Zuo, "Adaptive iterative generalized demodulation for nonstationary complex signal analysis: p," Science Press, Beijing, pp. 1–27, 2018.

[11] A. Grossmann and J. Morlet, "Decomposition of hardy functions into square integrable wavelets of constant shape," *SIAM Journal on Mathematical Analysis*, vol. 15, no. 4, pp. 723–736, 1984.

[12] N. T. Babu, H. S. Himamshu, P. N. Kumar, D. R. Prabha, and N. Chiluar, "Journal bearing fault detection based on Daubechies wavelet," *coustics*, vol. 42, no. 3, pp. 401–414, 2017.

[13] L. Ma, J. Kang, Y. Meng, and L. Lv, "Research on feature extraction of rolling bearing incipient fault based on Morlet wavelet transform [J]," *Chinese Journal of Scientific Instrument*, vol. 34, no. 04, pp. 920–926, 2013.

[14] R. Kumar and M. Singh, "Outer race defect width measurement in taper roller bearing using discrete wavelet transform of vibration signal," *Measurement*, vol. 46, no. 1, pp. 537–545, 2013.

[15] R. Lind, M. Brenner, and S. Haley, "Estimation of modal parameters using a wavelet-based approach," in *Proceedings of the AIAA atmospheric flight Mechanics conference*, vol. 97, p. 3836, New orleans, LA, USA, August 1997.

[16] Y. Zi, Q. Li, and Z. He, "Extraction of impulse response based on correlation filtering method of lapalace wavelet," *Journal of Vibration Engineering*, vol. 16, no. 1, pp. 67–70, 2003.

[17] H. Yang, J. Mathew, and L. Ma, "Fault diagnosis of rolling element bearings using basis pursuit," *Mechanical Systems and Signal Processing*, vol. 19, no. 2, pp. 341–356, 2005.

[18] H. Zhu, X. Wang, Y. Li, T. Liu, and M. Liu, "bearing fault diagnosis using orthogonal matching pursuit with pulse atoms based on vibration model," *Journal of Systems Science & Information*, vol. 229, no. 12, pp. 2303–2313, 2015.

[19] Z. Feng and M. Liang, "Complex signal analysis for planetary gearbox fault diagnosis via shift invariant dictionary learning," *Measurement*, vol. 90, pp. 382–395, 2016.

[20] W. Peng, D. Wang, C. Q. Shen, and D. N. Liu, "Sparse signal representations of bearing fault signals for exhibiting bearing fault features," *Shock and Vibration*, vol. 201612 pages, Article ID 1835127, 2016.

[21] Q. He, H. Song, and X. Ding, "Sparse signal reconstruction based on time-frequency manifold for rolling element bearing fault signature enhancement," *IEEE Transactions on Instrumentation and Measurement*, vol. 65, no. 2, pp. 482–491, 2016.

[22] M. B. Tang, "Vibration signal component separation by iteratively using basis pursuit and its application in mechanical fault detection [J]," *Journal of Sound and Vibration*, vol. 332, no. 20, pp. 5217–5235, 2013.

[23] G. Cai, S. Wang, Z. Zhu, W. Dai, and I. Selesnick, "Sparsity-enhanced signal decomposition via generalized minimax-concave penalty for gearbox fault diagnosis Science Direct," *Journal of Sound and Vibration*, vol. 432, no. 10, pp. 213–234, 2018.

[24] W. He, B. Chen, N. Zeng, and Y. Zi, "Sparsity-based signal extraction using dual Q-factors for gearbox fault detection," *ISA Transactions*, vol. 79, pp. 147–160, 2018.

[25] S. S. Chen, D. L. Donoho, and M. A. Saunders, "Atomic decomposition by basis pursuit," *SIAM Review*, vol. 43, no. 1, pp. 129–159, 2001.

[26] J. Yang, Y. Peng, X. Wenli, and Q. Dai, "Ways to sparse representation: a comparative study," *Tsinghua Science and Technology*, vol. 14, no. 4, pp. 434–443, 2009.

[27] J. A. Tropp and A. C. Gilbert, "Signal recovery from random measurements via orthogonal matching pursuit," *IEEE Transactions on Information Theory*, vol. 53, no. 12, pp. 4655–4666, 2007.

[28] R. Rubinstein, A. M. Bruckstein, and M. Elad, "Dictionaries for sparse representation modeling," *Proceedings of the IEEE*, IEEE, vol. 98, no. 6, pp. 1045–1057, 2010.

[29] A. M. Bruckstein, D. L. Donoho, and M. Elad, "From sparse solutions of systems of equations to sparse modeling of signals and images," *SIAM Review*, vol. 51, no. 1, pp. 34–81, 2009.

[30] B. K. Natarajan, "Sparse approximate solutions to linear systems," *SIAM Journal on Computing*, vol. 24, no. 2, pp. 227–234, 1995.

[31] S. Wang, W. Huang, and Z. K. Zhu, "Transient modeling and parameter identification based on wavelet and correlation filtering for rotating machine fault diagnosis," *Mechanical Systems and Signal Processing*, vol. 25, no. 4, pp. 1299–1320, 2011.

[32] W. A. Smith and R. B. Randall, "Rolling element bearing diagnostics using the Case Western Reserve University data: a benchmark study," *Mechanical Systems and Signal Processing*, vol. 64-65, pp. 100–131, 2015.

[33] Y. Yang, P. Fu, and Y. He, "bearing fault automatic classification based on deep learning," *IEEE Access*, vol. 6, pp. 71540–71554, 2018.